

Artificial Neural Networks for Quantum Sensing: Metrologically Resourceful State Detection

1st Uman Khalid

*Department of Electronics and
Information Convergence Engineering
Kyung Hee University
Yongin, Korea
umankhalid@khu.ac.kr*

2nd Trung Q. Duong

*Department of Electrical and
Computer Engineering
Memorial University of Newfoundland
St. John's, NL A1B 3X5, Canada
tduong@mun.ca*

3rd Hyundong Shin

*Department of Electronics and
Information Convergence Engineering
Kyung Hee University
Yongin, Korea
hshin@khu.ac.kr*

Abstract—The detection of fundamental quantum resources—namely coherence, discord, and entanglement—benchmarks the metrological power of quantum sensing networks. Traditional methods for certifying these resources, like exhaustive optimization-based tomographic procedures, are resource-intensive and vary significantly. This paper proposes a framework for identifying metrologically useful quantum sensing probes by detecting fundamental quantum resources. Herein, we introduce a witness-based certification method that is experimentally accessible and efficient, though it has limitations in reliability and universality. To address these, we employ artificial neural networks (ANNs) to classify quantum states into resourceful and resourceless states, enhancing the scope and reliability of proposed framework. The performance of ANN-based quantum state classification is also analyzed, positioning ANNs as effective tools for data-driven detection of metrologically resourceful states in quantum sensing tasks.

Index Terms—Quantum sensing networks, quantum metrology, artificial neural networks, quantum state classification.

I. INTRODUCTION

Quantum sensing and metrology utilize the distinct properties of quantum systems for highly precise measurements, exceeding classical limits [1]. By exploiting quantum resources, these tasks aim for achieving the Heisenberg limit through steps such as probe state preparation, sensing, readout, and estimation [2]. This process benefits from the inherent sensitivity of quantum systems to environmental changes, marking a significant advancement in measurement accuracy and efficiency.

Quantum resources such as coherence, discord, and entanglement are fundamental for enhancing the capabilities of quantum metrology tasks performed over quantum sensing networks [3]–[5]. These resources enable quantum probes to perform measurements with greater accuracy and precision than classical systems, finding applications in localization, tracking, and monitoring [6]. Moreover, the quantum resources provide distinct advantages, so seeking quantum states with profound application-specific usefulness in quantum sensing networks is critical. For instance, in quantum metrology tasks, discord captures minimum phase estimation accuracy, coherence impacts the unitary evolution speed limit for phase encoding, and entanglement permits exceeding classical limits of phase uncertainty [7]–[9]. This emphasizes how crucial it

is to discern between resourceful and resourceless quantum states in order to take advantage of benefits peculiar to certain applications in quantum sensing.

Identifying and classifying quantum states that exhibit quantum advantage in sensing and metrology is vital [10], [11]. The identification metrics detecting resourceful quantum states are not only key indicators of metrological resourcefulness but also quality metrics to benchmark the performance of quantum sensing networks [12]. Traditional detection techniques like quantum tomography face limitations due to the exponential increase in required measurements as system size grows, while the alternate methods like quantum witness lack in reliability and universality [13]–[15]. Additionally, environmental decoherence negatively impacts quantum resources, leading to the preparation of noisy probe states. This necessitates the exploration of new approaches, such as ANNs, for efficient and accurate classification of prepared quantum sensing probes, thereby facilitating the identification of metrologically resourceful probe states for advanced quantum sensing applications [16].

In this paper, we address the metrologically resourceful state detection problem by employing ANNs. First, we formulate quantum witnesses mechanism to certify resourceful quantum states. Then, we transform the certification task to classification task by virtue of ANNs. The performance analysis demonstrates that the proposed method significantly enhances the detection of metrologically resourceful states, improving both reliability and generality.

II. METROLOGICALLY RESOURCEFUL STATE DETECTION

In this section, we formulate metrologically resourceful state detection mechanism by utilizing quantum resource witnesses for coherence, discord, and entanglement. To enhance the reliability, robustness, and generality, we transform quantum resource witness task into quantum state classification by virtue of ANNs (as depicted in Fig. 1).

A. Metrologically Resourceful State Witnesses

Given a test quantum state, $d \times d$ density operator, the associated generalized Gell-Mann operators (GGO) basis rep-

resentation is

$$\rho = \frac{1}{d}I + \sqrt{\frac{d-1}{2d}} \mathbf{s} \cdot \boldsymbol{\sigma}, \quad (1)$$

where Bloch vector $\mathbf{s} = (\{s_{\text{sym}}^{j,k}\}, \{s_{\text{asym}}^{j,k}\}, \{s_{\text{diag}}^l\})$ with indices $1 \leq j < k \leq d$ and $1 \leq l \leq d-1$ such that $\|\mathbf{s}\| \leq 1$ and, a vector containing GGO as $\boldsymbol{\sigma} = (\{\sigma_{\text{sym}}^{j,k}\}, \{\sigma_{\text{asym}}^{j,k}\}, \{\sigma_{\text{diag}}^l\})$ having symmetric GGO $\sigma_{\text{sym}}^{j,k} = |j\rangle\langle k| + |k\rangle\langle j|$, anti-symmetric GGO $\sigma_{\text{asym}}^{j,k} = -\iota|j\rangle\langle k| + \iota|k\rangle\langle j|$ and diagonal GGO $\sigma_{\text{diag}}^l = \sqrt{\frac{2}{l(l+1)}} (\sum_{j=1}^l |j\rangle\langle j| - l|l+1\rangle\langle l+1|)$ [17]. The test state undergoes quantum operation described as a trace preserving map Φ^m and then subject to a quantum witness operator W^m . Quantum witness is a functional that distinguishes any specific quantum state from others. However, the optimal witness operators require exhaustive optimization for fine tuning of involved parameters [18]–[20]. Herein, without the loss of generality, employed witness operators are $d \times d$ Hermitian observable expressed in weighted standard GGO basis as $W^m = w_0 I + \mathbf{w}^m \cdot \boldsymbol{\sigma}$, where $w_i^m \in [-1, 1]$ [21], [22]. Thus, ushering random rotations of basis observables with regards to global measurements [23], [24]. The global measurement map projects the mapped test state to yield an expectation value which is a weighted sum of

$$b_i^m = \sqrt{\frac{d}{2(d-1)}} \text{tr}(\Phi^m(\rho)\sigma_i), \quad (2)$$

where $\text{tr}(\cdot)$ is the trace function and $m \in \{C, D, E\}$ indexes for relevant quantum resource, i.e., coherence, discord, and entanglement, respectively, under witness consideration. In most situations, only d values of b_i^m are sufficient, instead of $d^2 - 1$, to reliably detect the presence of quantum resources in unknown quantum states [25]. In other words, these fundamental resources are evaluated as a function of the expectation values b_i^m of a set of observables $\{\sigma_i\}$ for a mapped test state. These mathematical functions produce real values that depend on the presence of relevant quantum resource in the test state, enabling the construction of corresponding quantum resource witness inequality. The detection rules set for these inequalities certify inherent quantum resource. The detection mechanisms for coherence, discord, and entanglement are detailed as follows.

a) Coherence Witness: For a test state, coherence witness operators are traceless Hermitian operators given by $W^C = \mathbf{w}^C \cdot \boldsymbol{\sigma}$, where $\mathbf{w}^C = (\{w_{\text{sym}}^{j,k}\}, \{w_{\text{asym}}^{j,k}\}, \{0\})$ [26]. The vectors $\mathbf{w}^{C, (j,k)} = (w_{\text{sym}}^{j,k}, w_{\text{asym}}^{j,k})$ satisfy normalization condition $\|\mathbf{w}^{C, (j,k)}\| = 1$. Herein, Φ^C denotes an incoherent unitary completely positive trace preserving map. In terms of operator-sum representation, the transformation is described as $\Phi^C(\rho) = \sum_i K_i \rho K_i^\dagger$, provided $\sum_i K_i^\dagger K_i = I$. For an incoherent test state, there exists an additional requirement as $K_i \rho K_i^\dagger / \text{tr}(K_i \rho K_i^\dagger) \in \mathcal{I}$, whereas the set \mathcal{I} consists of all incoherent states. The quantum coherence witness inequality based coherence detection criteria is presented as

$$C_W = \text{tr}(\Phi^C(\rho)W^C) \neq 0, \quad (3)$$

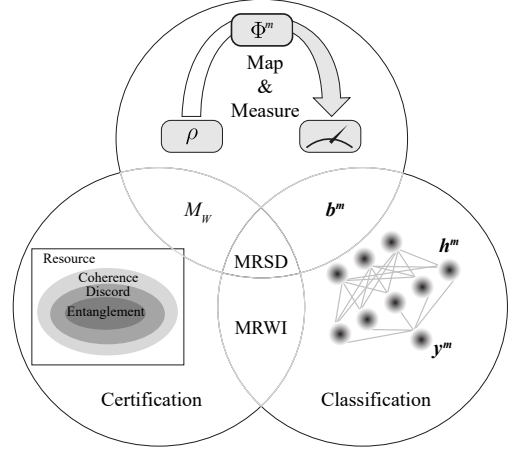


Fig. 1. A Venn diagram illustration for the proposed formalism of metrologically resourceful state detection (MRSD): A test state ρ undergoes a trace preserving map Φ^m and witness measurement W^m to obtain linear combination of expectation values b_i^m to instantiate corresponding metrological resource witness inequality (MRWI). The detection rules set for such inequalities imply whether test state is coherent/discordant/entangled or not. On one hand, expectation values in $M_W \in \{C_W, D_W, E_W\}$ are processed to quantify corresponding quantum resource. On the other hand, these values are fed into ANNs to build coherent-incoherent/discordant-non discordant/entangled-separable state classifiers.

for a coherent state where the equality is attained only for an incoherent state. Any nonzero value in b^C manifests coherence. Therefore, atleast one measurement is necessary to detect coherence while detection accuracy can be further enhanced by incorporating all $d^2 - d$ expectation values. So, arbitrary choice of witness coefficients already provides a partial solution to the coherence witness. This approach outclasses standard state tomography wherein d^2 observables are critical in detecting coherence in an unknown state, after reconstructing the $d \times d$ density matrix.

b) Discord Witness: For a test state, discord witness operators are traceless Hermitian operators realized via linear combination of symmetric and anti-symmetric GGO as $W^D = \mathbf{w}^D \cdot \boldsymbol{\sigma}$, where $\mathbf{w}^D = (\{w_{\text{sym}}^{D, (j,k)}\}, \{w_{\text{asym}}^{D, (j,k)}\}, \{0\})$ satisfying $\|\mathbf{w}^D\| \leq 1$. Herein, Φ^D is a local incoherent unitary transformation map. Therefore, symmetric discord detection criteria based on discord witness inequality is formulated as

$$D_W = \text{tr}(\Phi^D(\rho)W^D) \neq 0, \quad (4)$$

for a discordant state, whereas equality is obtained only for a completely nondiscordant state. In short, any nonzero significant value in b^D hints at the presence of discord. The detection confidence is increased by employing all nonzero values from total $d^2 - d$ expectation values.

c) Entanglement Witness: For a test state, the corresponding normalized entanglement witness operator is given as $W^E = (\frac{1}{d} + \frac{\zeta}{2} \mathbf{w}^E \cdot \boldsymbol{\sigma})$, where $\mathbf{w}^E = (\{w_{\text{sym}}^{j,k}\}, \{w_{\text{asym}}^{j,k}\}, \{w_{\text{diag}}^l\})$ and $\zeta = \sqrt{\frac{2(d-1)}{d}}$. It is noteworthy that $\|\mathbf{w}^E\| \leq 1$ corresponding to $\text{tr}(W^E) = 1$. Φ^E is non completely positive trace preserving map. For entanglement

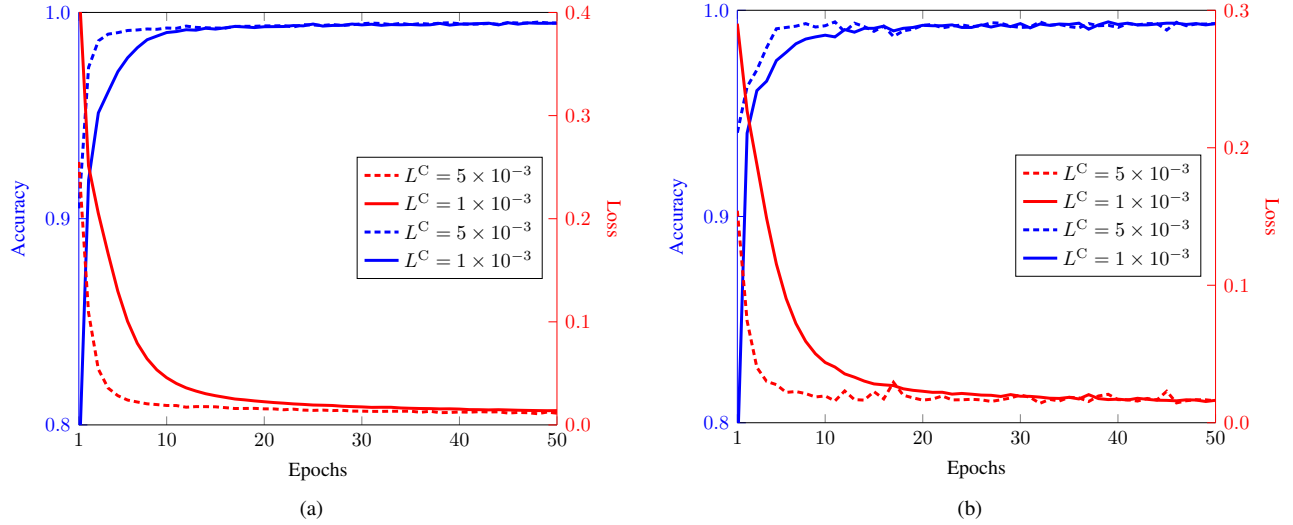


Fig. 2. Performance evaluation of coherent-incoherent classifier: (a) Training and (b) validation accuracy/loss plotted as a functions of epochs for $N_h^C = 40$.

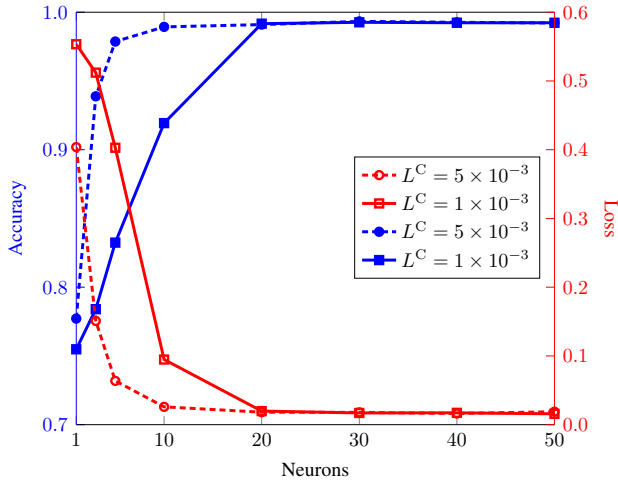


Fig. 3. Testing accuracy/loss plotted as a function of N_h^C , i.e., the number of neurons in the hidden layer.

detection, the entanglement witness inequality is constructed as

$$E_W = \text{tr}(\Phi^E(\rho)W^E) < 0, \quad (5)$$

wherein the inequality is violated only by separable state.

The effectiveness and reliability of tasks involving the witnessing of metrologically useful states hinge on the acquisition of optimal witness operators for the test states. The process of finding these optimal quantum witness operators for state discrimination is exhaustive. This difficulty stems from the requirement to traverse a complex optimization space, adhering to stringent mathematical and quantum mechanical criteria, such as the Hermiticity of operators and their ability to discriminate distinct states. A key stipulation is that the optimization encompasses the entirety of the state space, expanding exponentially with the quantum system's qubit count. Consequently, there is a significant increase in the demand

for computational resources, spanning both classical computational means for the execution of optimization algorithms and quantum mechanisms for the practical deployment and evaluation of prospective witness operators.

B. Metrologically Resourceful State Classifiers

Herein, we utilize ANNs to establish binary classifiers to distinguish metrologically resourceful quantum states from metrologically resourceless quantum states.

1) *ANN for Data-driven Detection*: The vectors \mathbf{b}^m are fed to ANN input layer as features. The model architecture has one hidden layer having each hidden neuron activated via a nonlinear yet faster to compute, ReLU function. This hidden layer transforms input feature vector to yield $\mathbf{h}^m = ([\boldsymbol{\eta}_1 \mathbf{b}^m + \xi_1]^+, \dots, [\boldsymbol{\eta}_{N_h^m} \mathbf{b}^m + \xi_{N_h^m}]^+)$, where N_h^m is the number of neurons in the hidden layer. The output layer is fixed at one neuron activated via sigmoid function to produce

$$\hat{y}^m = \frac{1}{1 + \exp\{-\mathbf{G} \cdot \mathbf{h}^m + g\}}, \quad (6)$$

such that the network parameters $\boldsymbol{\eta}_i, \mathbf{G}, \xi_i, g$ are randomly initialized and trained thoroughly. The implementation of ANN architecture is carried out on neural network sequential API keras. Binary cross-entropy is chosen as a loss function for binary classification while optimizer is Adam with default hyper parameters but varying learning rate L^m .

2) *Labeled Dataset Generation*: The quality, diversity, and size of corresponding master data sets \mathcal{D}^m are the main factors in effective training, validation, and testing the generalization performance of the model. The quality of data sets is maintained through noise-free witness measurements and correct labeling. The binary labeling of data for coherence, discord, and entanglement is achieved via their bonafide quantifiers as robustness of coherence, local quantum uncertainty, and negativity, respectively [3], [18], [27]. The cost of accurate labeling of data is removed in unsupervised learning case, but

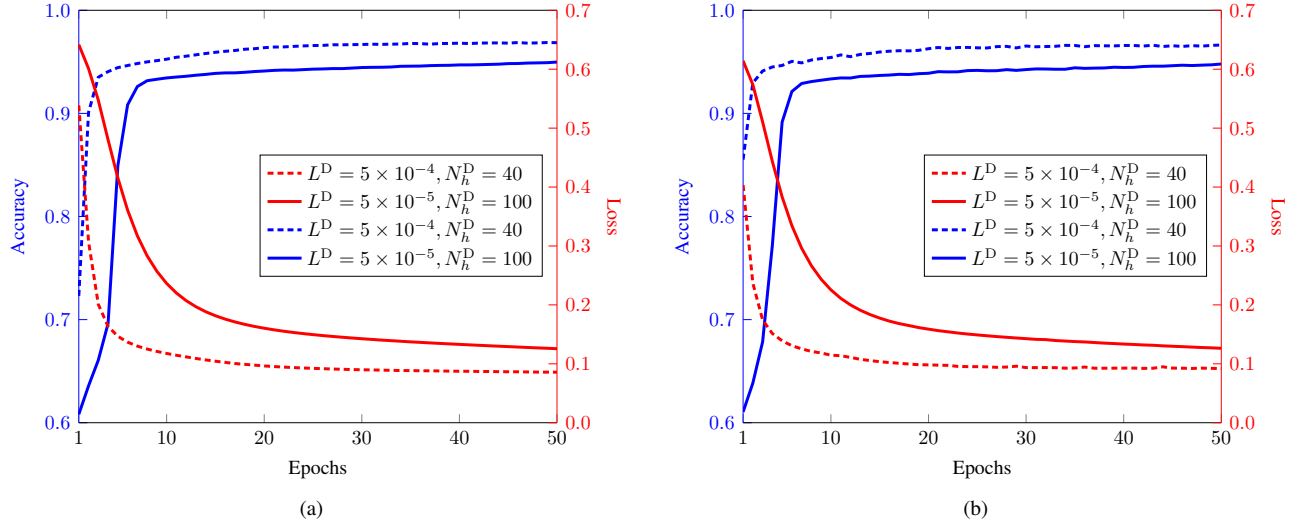


Fig. 4. Performance evaluation of discordant-non discordant classifier: (a) Training and (b) validation accuracy/loss plotted as a functions of epochs.

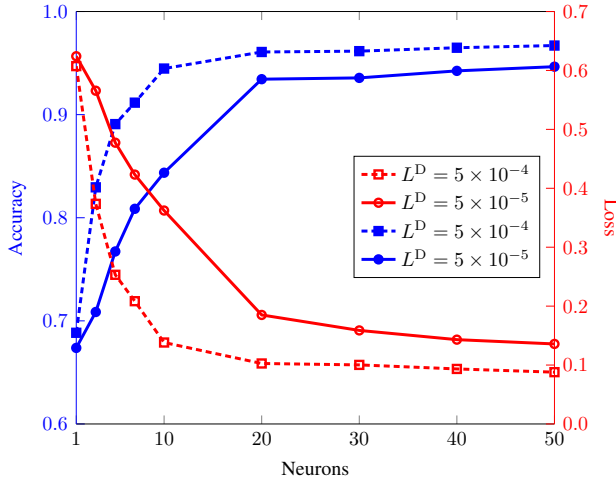


Fig. 5. Testing accuracy/loss plotted as a function of N_h^D , i.e., the number of neurons in the hidden layer.

at the expense of classification accuracy and increased size of data sets [28]. To avoid bias, approximately equal ratio of coherent and incoherent, discordant and non discordant, and entangled and separable states are generated for master datasets \mathcal{D}^m having large sizes N^m . The datasets are formed by incorporating a diverse range of resourceful-resourceless quantum states. Such data diversity is faithfully reflected in the ability of classifiers to generalize well to new unseen quantum states. The generation of quantum states and the map and measure operations are carried out using the functions of the QETLAB package (MATLAB based toolbox to explore the theory of quantum entanglement). The composition of datasets are detailed as follows.

a) *Coherence-Incoherence Dataset*: For \mathcal{D}^C having $N^C = 3 \times 10^4$, the data set comprises of 10^4 samples of random density matrices (RDM) having arbitrary rank

r , 10^4 samples of RDM having $r = 1$ decohered under global depolarizing noise, and 10^4 samples of RDM having $r = 4$ decohered under global depolarizing noise with noise parameter $p < 0.1$.

b) *Discord-Non Discord Dataset*: For \mathcal{D}^D having $N^D = 8 \times 10^4$, the data set comprises of 2×10^4 samples of RDM having arbitrary r , 2×10^4 samples of depolarized RDM having arbitrary r and p , 2×10^4 samples of product RDM, i.e., $(\rho_A \otimes \rho_B)$, and 2×10^4 samples of maximally discordant mixed states.

c) *Entanglement-Separability Dataset*: For \mathcal{D}^E having $N^E = 1.5 \times 10^5$, the data set comprises of 2×10^4 samples of RDM for each r , 2×10^4 samples of product RDM, 2×10^4 samples of depolarized RDM having $r = 1$, and 10^4 samples of depolarized RDM for each $r = 2, 3$, and 4 with arbitrary noise strength p .

3) *Classifiers Performance*: The labeled master data sets are divided into training, validation, and test sets in the ratio (0.64, 0.16, 0.2). Accuracy and loss are employed as metrics to evaluate the performance of resourceful-resourceless quantum state classifier models during training, validation, and testing process.

a) *Coherence-Incoherence Classifier*: Fig. 2(a) shows the trainability of ANN model in quantum coherence classification wherein train accuracy and loss smoothly converge to approximately 99.5% and 1% for $N_h^C = 40$. Fig. 2(b) validates the aforementioned trained model wherein validation accuracy is slightly less and validation loss is slightly more than the corresponding training metrics for new and unseen coherent-incoherent data instances. Testing metrics exhibit significant performance enhancement upon increasing the number of neurons in the hidden layer N_h^C , as depicted in Fig. 3. Herein, test accuracy and loss converge to approximately 98% and 2% at around $N_h^C = 20$.

b) *Discord-Non Discord Classifier*: Fig. 4(a) shows the training results of simple ANN model in quantum discord

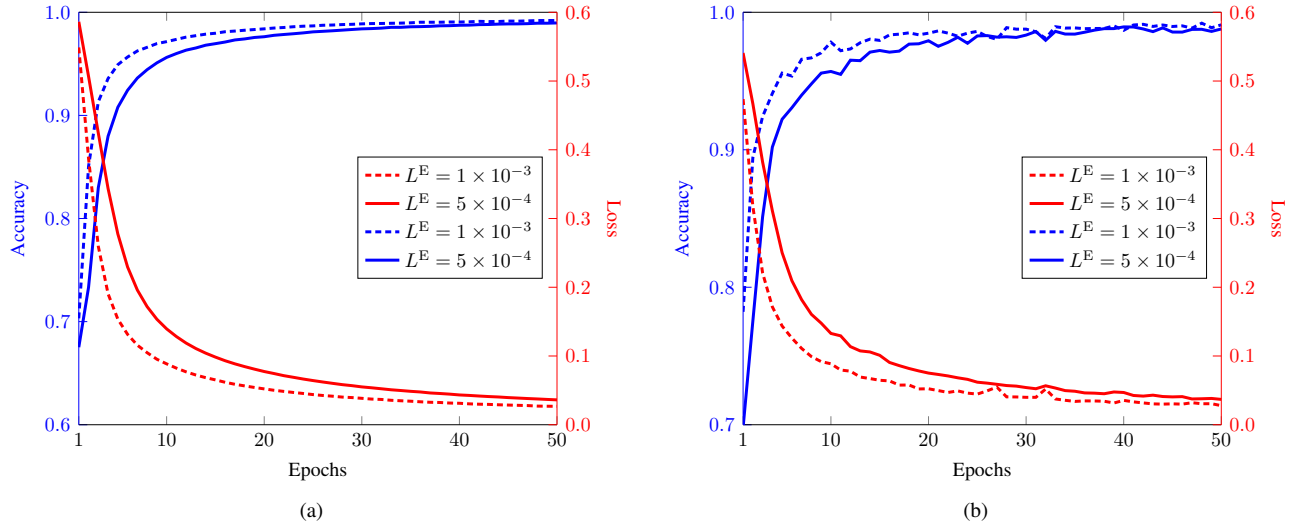


Fig. 6. Performance evaluation of entangled-separable classifier: (a) Training and (b) validation accuracy/loss plotted as a functions of epochs for $N_h^E = 300$.

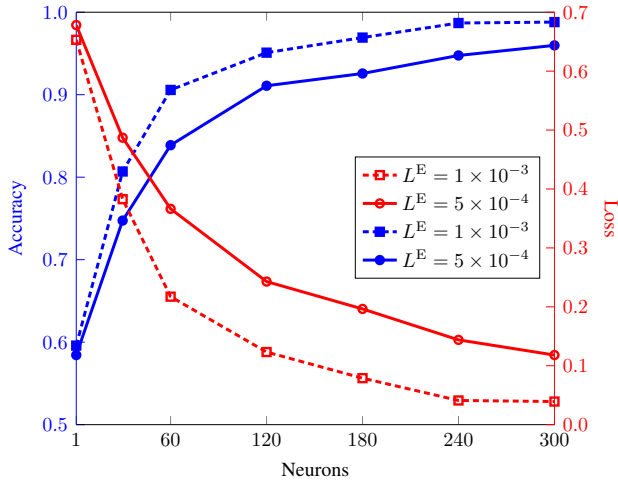


Fig. 7. Testing accuracy/loss plotted as a function of N_h^E , i.e., the number of neurons in the hidden layer.

classification wherein train accuracy fast converges to approximately 97% for $L^D = 5 \times 10^{-4}$ employing only $N_h^D = 40$ and 95% for $L^D = 5 \times 10^{-5}$ employing $N_h^D = 100$. Similarly, train loss converges to approximately 8.5% for $L^D = 5 \times 10^{-4}$ and 12.5% for $L^D = 5 \times 10^{-5}$. Fig. 4(b) validates the aforementioned trained model wherein validation accuracy is slightly less and validation loss is slightly more than the corresponding training metrics for new and unseen discordant-non discordant data instances. Classification performance improves by increasing the number of neurons in the hidden layer N_h^D , as depicted in Fig. 5. Herein, test accuracy and loss converge to approximately 96% and 10% at around $N_h^D = 20$ for $L^D = 5 \times 10^{-4}$ whereas 94% and 14% at around $N_h^D = 40$ for $L^D = 5 \times 10^{-5}$.

c) *Entanglement-Separability Classifier*: Fig. 6(a) shows the training curves of ANN model in quantum entanglement

classification wherein train accuracy smoothly converges to approximately 99% for $N_h^E = 300$. Similarly, train loss converges to approximately 2% for $L^E = 1 \times 10^{-3}$ and 3% for $L^E = 5 \times 10^{-4}$. Fig. 6(b) validates the aforementioned trained model wherein validation accuracy is slightly less and validation loss is slightly more than the corresponding training metrics for new and unseen entangled-separable data instances. Testing metrics exhibit significant performance enhancement upon increasing the number of neurons in the hidden layer N_h^E , as depicted in Fig. 7. However, test accuracy and loss reach 98% and 4% for $L^E = 1 \times 10^{-3}$ and 96% and 11% for $L^E = 5 \times 10^{-4}$ at $N_h^E = 300$.

III. CONCLUSION

In this work, we established a simple, robust, and reliable framework for identifying metrologically useful quantum sensing probes. By leveraging ANNs, we bridge supervised learning with quantum information science, achieving high accuracy in distinguishing resourceful from resourceless quantum states. This indicates ANNs' crucial role in quantum sensing tasks, enhancing metrologically resourceful state detection where traditional methods become inefficacious and unreliable.

ACKNOWLEDGMENT

This work was supported by the National Research Foundation of Korea (NRF) grant funded by the Korean government (MSIT) (NRF-2022R1A4A3033401) and by the MSIT (Ministry of Science and ICT), Korea, under the ITRC (Information Technology Research Center) support program (IITP-2024-2021-0-02046) supervised by the IITP (Institute for Information & Communications Technology Planning & Evaluation).

REFERENCES

- [1] U. Khalid, J. u. Rehman, S. N. Paing, H. Jung, T. Q. Duong, and H. Shin, "Quantum network engineering in the NISQ age: Principles, missions, and challenges," *IEEE Netw.*, early access.

- [2] U. Khalid, Y. Jeong, and H. Shin, "Measurement-based quantum correlation in mixed-state quantum metrology," *Quantum Inf. Process*, vol. 17, no. 12, p. 343, Nov. 2018.
- [3] R. Horodecki, P. Horodecki, M. Horodecki, and K. Horodecki, "Quantum entanglement," *Rev. Mod. Phys.*, vol. 81, no. 2, p. 865, Jun. 2009.
- [4] A. Streltsov, G. Adesso, and M. B. Plenio, "Colloquium: Quantum coherence as a resource," *Rev. Mod. Phys.*, vol. 89, no. 4, p. 041003, Oct. 2017.
- [5] A. Bera, T. Das, D. Sadhukhan, S. S. Roy, A. S. De, and U. Sen, "Quantum discord and its allies: A review of recent progress," *Rep. Prog. Phys.*, vol. 81, no. 2, p. 024001, Dec. 2017.
- [6] U. Khalid, M. S. Ulum, A. Farooq, T. Q. Duong, O. A. Dobre, and H. Shin, "Quantum semantic communications for Metaverse: Principles and challenges," *IEEE Wireless Commun.*, vol. 30, no. 4, pp. 26–36, Aug. 2023.
- [7] D. Girolami, A. M. Souza, V. Giovannetti, T. Tufarelli, J. G. Filgueiras, R. S. Sarthour, D. O. Soares-Pinto, I. S. Oliveira, and G. Adesso, "Quantum discord determines the interferometric power of quantum states," *Phys. Rev. Lett.*, vol. 112, no. 21, p. 210401, May 2014.
- [8] I. Marvian, R. W. Spekkens, and P. Zanardi, "Quantum speed limits, coherence, and asymmetry," *Phys. Rev. A*, vol. 93, no. 5, p. 052331, May 2016.
- [9] U. Khalid, J. ur Rehman, and H. Shin, "Metrologically resourceful multipartite entanglement under quantum many-body effects," *Quantum Sci. Technol.*, vol. 6, no. 2, p. 025007, Jan. 2021.
- [10] N. Asif, U. Khalid, A. Khan, T. Q. Duong, and H. Shin, "Entanglement detection with artificial neural networks," *Sci. Rep.*, vol. 13, no. 1, p. 1562, Jan. 2023.
- [11] S. Lu, S. Huang, K. Li, J. Li, J. Chen, D. Lu, Z. Ji, Y. Shen, D. Zhou, and B. Zeng, "Separability-entanglement classifier via machine learning," *Phys. Rev. A*, vol. 98, p. 012315, Jul. 2018.
- [12] E. Chitambar and G. Gour, "Quantum resource theories," *Rev. Mod. Phys.*, vol. 91, no. 2, p. 025001, Apr. 2019.
- [13] J. Eisert, D. Hangleiter, N. Walk, I. Roth, D. Markham, R. Parekh, U. Chabaud, and E. Kashefi, "Quantum certification and benchmarking," *Nat. Rev. Phys.*, vol. 2, no. 7, pp. 382–390, Jul. 2020.
- [14] J. Roik, K. Bartkiewicz, A. Černoch, and K. Lemr, "Accuracy of entanglement detection via artificial neural networks and human-designed entanglement witnesses," *Phys. Rev. Applied*, vol. 15, p. 054006, May 2021.
- [15] N. H. Nguyen, E. C. Behrman, M. A. Moustafa, and J. E. Steck, "Benchmarking neural networks for quantum computations," *IEEE Trans. Neural Netw. Learn. Syst.*, vol. 31, no. 7, pp. 2522–2531, Jul. 2020.
- [16] E. C. Behrman, R. E. F. Bonde, J. E. Steck, and J. F. Behrman, "On the correction of anomalous phase oscillation in entanglement witnesses using quantum neural networks," *IEEE Trans. Neural Netw. Learn. Syst.*, vol. 25, no. 9, pp. 1696–1703, Sept. 2014.
- [17] R. A. Bertlmann and P. Krammer, "Bloch vectors for qudits," *J. Phys. A: Math. Theor.*, vol. 41, no. 23, p. 235303, May 2008.
- [18] C. Napoli, T. R. Bromley, M. Cianciaruso, M. Piani, N. Johnston, and G. Adesso, "Robustness of coherence: An operational and observable measure of quantum coherence," *Phys. Rev. Lett.*, vol. 116, no. 15, p. 150502, Apr. 2016.
- [19] R. Auccaise, J. Maziero, L. C. Céleri, D. O. Soares-Pinto, E. R. deAzevedo, T. J. Bonagamba, R. S. Sarthour, I. S. Oliveira, and R. M. Serra, "Experimentally witnessing the quantumness of correlations," *Phys. Rev. Lett.*, vol. 107, p. 070501, Aug. 2011.
- [20] F. G. S. L. Brandão, "Quantifying entanglement with witness operators," *Phys. Rev. A*, vol. 72, no. 2, p. 022310, Aug. 2005.
- [21] Y.-T. Wang, J.-S. Tang, Z.-Y. Wei, S. Yu, Z.-J. Ke, X.-Y. Xu, C.-F. Li, and G.-C. Guo, "Directly measuring the degree of quantum coherence using interference fringes," *Phys. Rev. Lett.*, vol. 118, no. 2, p. 020403, Jan. 2017.
- [22] M. Ringbauer, T. R. Bromley, M. Cianciaruso, L. Lami, W. S. Lau, G. Adesso, A. G. White, A. Fedrizzi, and M. Piani, "Certification and quantification of multilevel quantum coherence," *Phys. Rev. X*, vol. 8, no. 4, p. 041007, Oct. 2018.
- [23] M. Păni, A. Kalev, D. Padilha, and B. Ruck, "Estimating expectation values using approximate quantum states," *Quantum*, vol. 5, p. 413, Mar. 2021.
- [24] B. Dirkse, M. Pompili, R. Hanson, M. Walter, and S. Wehner, "Witnessing entanglement in experiments with correlated noise," *Quantum Sci. Technol.*, vol. 5, no. 3, p. 035007, Jun. 2020.
- [25] S. T. Flammia and Y.-K. Liu, "Direct fidelity estimation from few Pauli measurements," *Phys. Rev. Lett.*, vol. 106, no. 23, p. 230501, Jun. 2011.
- [26] H. Ren, A. Lin, S. He, and X. Hu, "Quantitative coherence witness for finite dimensional states," *Ann. Phys.*, vol. 387, pp. 281–289, Oct. 2017.
- [27] D. Girolami, T. Tufarelli, and G. Adesso, "Characterizing nonclassical correlations via local quantum uncertainty," *Phys. Rev. Lett.*, vol. 110, p. 240402, Jun. 2013.
- [28] Y. Chen, Y. Pan, G. Zhang, and S. Cheng, "Detecting quantum entanglement with unsupervised learning," *Quantum Sci. Technol.*, vol. 7, no. 1, p. 015005, Nov. 2021.